Spikey: Self-Lensing Flares from Eccentric SMBH Binaries

Betty X. Hu[1,2⋆], Daniel J. D'Orazio[3], Zoltán Haiman[4], Krista Lynne Smith[5], Bradford Snios[6], Maria Charisi[7], Rosanne Di Stefano[6]

[1]*Department of Physics, Harvard University, 17 Oxford Street, Cambridge, MA 02138, USA*
[2]*Department of Applied Physics and Applied Math, Columbia University, 500 West 120th Street, New York, NY 10027, USA*
[3]*Institute for Theory and Computation, Harvard University, 60 Garden Street, Cambridge, MA 02138, USA*
[4]*Department of Astronomy, Columbia University, 550 West 120th Street, New York, NY 10027, USA*
[5]*Stanford University KIPAC, SLAC, Menlo Park, CA 94025, USA*
[6]*Harvard-Smithsonian Center for Astrophysics, 60 Garden Street, Cambridge, MA 02138, USA*
[7]*TAPIR, California Institute of Technology, 1200 East California Blvd, Pasadena, CA 91125, USA*

9 May 2020

ABSTRACT

We examine the light curves of two quasars, motivated by recent suggestions that a supermassive black hole binary (SMBHB) can exhibit sharp lensing spikes. We model the variability of each light curve as due to a combination of two relativistic effects: the orbital relativistic Doppler boost and gravitational binary self-lensing. In order to model each system we extend previous Doppler plus self-lensing models to include eccentricity. The first quasar is identified in optical data as a binary candidate with a 20-yr period (Ark 120), and shows a prominent spike. For this source, we rule out the lensing hypothesis and disfavor the Doppler-boost hypothesis due to discrepancies in the measured vs. recovered values of the binary mass and optical spectral slope. The second source, which we nickname Spikey, is the rare case of an active galactic nucleus (AGN) identified in Kepler's high-quality, high-cadence photometric data. For this source, we find a model, consisting of a combination of Doppler modulation and a narrow symmetric lensing spike, consistent with an eccentric SMBHB with mass $M_{\rm tot} = 3 \times 10^7 M_\odot$, rest-frame orbital period $T = 418$ days, eccentricity $e = 0.5$, and seen at an inclination 8° from edge-on. This interpretation can be tested by monitoring Spikey for periodic behavior and recurring flares in the next few years. In preparation for such monitoring we present the first X-ray observations of this object taken by the Neil Gehrels Swift observatory.

Key words: gravitational lensing: micro, quasars: supermassive black holes

1 INTRODUCTION

Motivated by the knowledge that supermassive black holes (SMBHs) are found in the nuclei of most massive galaxies in the universe and that galaxies often merge (Kormendy & Ho 2013; Richstone et al. 1998), one expects supermassive black hole binaries (SMBHBs) to be commonly found at the center of galaxies (Begelman et al. 1980). Despite this, very few SMBHBs have been detected, typically at separations of several kpc (*e.g.*, Dotti et al. 2012; Comerford et al. 2013). Recently, quasars with periodically varying optical emission have been examined as candidates for SMBHBs (Graham et al. 2015; Charisi et al. 2016; Liu et al. 2019). Such periodic variability may be imprinted by the orbital motion of a sub-pc separation SMBHB via time variable accretion (*e.g.*, Artymowicz & Lubow 1994; Hayasaki et al. 2007; MacFadyen & Milosavljević 2008; Cuadra et al. 2009; Shi et al. 2012; D'Orazio et al. 2013; Farris et al. 2014; D'Orazio et al. 2015a; Shi & Krolik 2015; Muñoz & Lai 2016; Bowen et al. 2019), or by the relativistic Doppler boost (D'Orazio et al. 2015b). It has also been suggested that binary self-lensing, which would occur if the accretion flow from one black hole was gravitationally lensed by its partner, could serve as a signature of SMBHBs (D'Orazio & Di Stefano 2018, hereafter D18). Periodic self-lensing is expected in a non-negligible number of SMBHBs if at least one black hole is accreting, and is most dramatic in systems with small orbital inclinations relative to the line of sight. The resulting lensing flare is symmetric and encodes the binary orbital parameters; periodic repetition of such a flare would be a unique signature of a sub-pc separation SMBHB.

In this paper, we extend the models of D18 to include orbital eccentricity. We then use these models to analyze two SMBHB candidates by considering periodically varying continuum emission caused by the relativistic Doppler boost in addition to flares from periodic self-lensing. We choose to consider continuum variability due to the Doppler boost instead of (or in addition to) variable accretion because the former, without introducing extra model parameters, provides a unique signature when combined with the lensing flares (see D18 and D'Orazio & Di Stefano 2019). Additionally, in the case of favorably aligned systems, both effects are required to occur via relativity alone.

We save a rigorous search for self-lensing flares in existing

⋆ bhu@g.harvard.edu; daniel.dorazio@cfa.harvard.edu, zoltan@astro.columbia.edu

time-domain data for a future endeavor, and here consider two individually identified Doppler + lensing candidates. One is the result of long term optical monitoring, and the other a by-product of the Kepler mission. We find that our Doppler + self-lensing model provides an excellent fit for the light curve of an active galactic nucleus (AGN) identified in Kepler's data. We use our model to predict when the putative next lensing flares will occur, providing us with a clear test of the binary hypothesis for the Kepler AGN.

2 CANDIDATE BINARIES

We first consider Arakelian 120 (hereafter Ark 120), a nearby radio-quiet type 1 AGN at a distance of 143 Mpc (z = 0.03271). Spectroscopic and photometric data of this source exists from 1974 up to 2017. As reported in Li et al. (2019), long-term variations in the light curves of V-band flux densities, 5100 $\AA$ flux densities, and $H\beta$ integrated fluxes exhibit a sinusoidal pattern with a $\sim$ 20 year period. In addition, the binned, merged light curve of V-band and 5100 $\AA$ flux densities, shown in Figure 3, show two significant peaks around 1982 and 1997 (MJD $\sim$ 45,000 and 51,000, respectively), which we considered to be suggestive of binary self-lensing. We note that while this system has been put forward as a SMBHB candidate based upon observed periodic variability, this periodicity thus far spans only two cycles, and correlated noise processes intrinsic to AGN can mimic such periodicity for small numbers of observed cycles if the correlation time of the noise is of order the temporal baseline of observations or longer (Vaughan et al. 2016). In this work we aim simply to test whether or not the observed sinusoidal variations and peaks in the light curve could be caused by a SMBHB Doppler boost plus self-lensing model.

While by eye, the sinusoidal nature of the Ark 120 light curve is suggestive of a putative binary orbit with modest eccentricity – the first peak being located near the mean of the sinusoidal portion of the light curve – the location of the second peak, below the mean, motivates us to consider eccentric orbits.

We next considered KIC 11606854 (hereafter "Spikey"), the rare case of a type 1 AGN identified in Kepler's high-quality, high-cadence photometric data. Kepler was launched by NASA to detect Earth-sized and smaller exoplanets in or near habitable zones by searching for transits in stellar light curves. Although only 7 AGN were known to be in Kepler's field of view (FOV) prior to the start of the mission, in recent years, efforts by various groups (Carini & Ryle 2012; Edelson & Malkan 2012) have led to dozens of AGN being discovered in the Kepler FOV. [1] Spikey was identified in Smith et al. (2018) by its striking symmetric flare in the center of a rising continuum (Figure 4). While Spikey does not exhibit a periodic light curve, by eye, the non-sinusoidal shape of the light curve and location of the flare imply a high-eccentricity orbit within the Doppler + self-lensing model, which we test below. Spikey is a high-z source, at z = 0.918.

[1] Analysis has also been done on these Kepler AGN in recent years: Kasliwal et al. (2015) tests the popular damped random walk (DRW) model of AGN variability (MacLeod et al. 2010; Kozłowski et al. 2010) and finds that less than half the objects considered are consistent with a DRW, and Smith et al. (2018) offers a comprehensive analysis of 21 light curves, power spectral density functions (PSDs), and flux histograms, examining the data for correlations with various physical parameters.

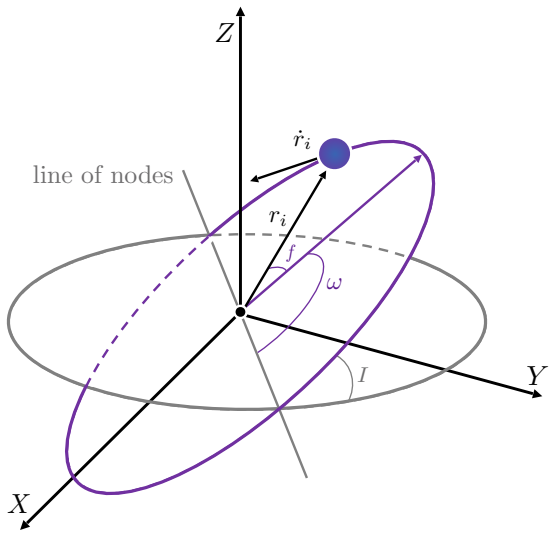

Figure 1.

Orbital parameters as described in section 3.1, with the Z-axis oriented towards the observer. $\mathbf{r_i}$ is the vector from the center of mass to the i-th mass, $\dot{\mathbf{r}}_\mathbf{i}$ the velocity vector, ω the argument of periapse, f the true anomaly, and I the inclination.

3 MODEL DESCRIPTION

3.1 Model Components

In addition to a steady mean flux F_0, we consider four components in our light curve model: the Doppler boost, gravitational microlensing, stochastic noise described by the damped random walk (DRW) model, and photometric noise,

$$F_{\rm obs} = F_0 \times (1 + \Delta F_{\rm Doppler}) \times (1 + \Delta F_{\rm lensing}) \times (1 + \Delta F_{\rm DRW}) + \Delta F_{\rm photometric}. \quad (1)$$

For small Δ, we can ignore second and third-order terms between the DRW noise and relativistic effects, giving,

$$F_{\rm obs} = F_0 \times (1 + \Delta F_{\rm Doppler}) \times (1 + \Delta F_{\rm lensing}) + \Delta F_{\rm DRW} + \Delta F_{\rm photometric}. \quad (2)$$

A widely used model for stochastic quasar variability in the optical wavelength range is the damped random walk (DRW) model (Kozłowski et al. 2010; MacLeod et al. 2010). DRW variability follows correlated random Gaussian fluctuations that can be described by two scales: τ, the damping or characteristic time scale, and σ, the long-term standard deviation of variability. The asymptotic value of the structure function SF_∞, which measures the mean value of the flux variance for measurements $x(t)$ separated by a given time interval Δt (Hughes et al. 1992), at large Δt, is related to the σ parameter as $\mathrm{SF}_\infty = \sqrt{2}\sigma$. We adopt τ and SF_∞ as the two main stochastic quasar variability model parameters. The power spectral density (PSD) for the DRW is then given by,

$$\mathrm{PSD}(f) = \frac{\tau^2 \mathrm{SF}_\infty^2}{1 + (2\pi f \tau)^2}. \quad (3)$$

The DRW has a PSD $\propto f^{-2}$, corresponding to red noise at high frequencies ($f > (2\pi\tau)^{-1}$), flattening to a constant, white noise, at low frequencies ($f < (2\pi\tau)^{-1}$). The break frequency is defined as $(2\pi\tau)^{-1}$, where SF(Δt) flattens to SF_∞.

The relativistic Doppler boost as a cause of periodicity in

SMBHBs is discussed in the case of quasar PG 1302-102 in D'Orazio et al. (2015b), and in the case of the periodic-light-curve SMBHB candidates in Charisi et al. (2018). D'Orazio et al. (2015b) proposes that because optical and UV emissions likely arise from gas bound to the individual BHs, the luminosity of the brighter mini-disk (typically that of the faster moving secondary SMBH) would be Doppler boosted, with the Doppler-induced variability being dominant to hydrodynamically-introduced fluctuations in unequal-mass binaries (D'Orazio et al. 2016). Because the number of photons, proportional to F_ν/ν^3 with F_ν the apparent flux at a fixed observed frequency ν, is Lorentz invariant, it follows that F_ν is modified from the flux of a stationary source F^0_ν. Defining $D = [(1-\beta^2)^{-1/2}(1-\beta_\parallel)]^{-1}$, with $\beta = v/c$, c the speed of light, and $\beta_\parallel$ the component along the line of sight, and assuming an intrinsic power-law spectrum $F^0_\nu \propto \nu^\alpha$, the apparent flux at a fixed observed frequency is modified to $F_\nu = D^3 F^0_{D^{-1}\nu} = D^{3-\alpha} F_0$. To first order in β, this causes a modulation of F_ν by a fractional amplitude $\Delta F_\nu/F_\nu = \pm(3-\alpha)(v/c)\cos\phi \sin I$, with I, ϕ, and v the orbital inclination ($I = \pi/2$ denoting an edge-on binary), phase, and three-dimensional velocity. .

Murray & Correia (2010) gives the radial velocity, the projection of the velocity vector onto the line of site, as:

$$v_{r,i} = \dot{\mathbf{r}}_\mathbf{i} \cdot \hat{\mathbf{Z}} = V_Z + K_i(\cos(\omega + f) + e\cos\omega), \tag{4}$$

where the subscript i denotes the $i^{\rm th}$ binary component, $\mathbf{r_1}$ denotes the vector from the center of mass to the more massive primary, the Z-axis is oriented toward the observer, $V_Z = \mathbf{V} \cdot \hat{\mathbf{Z}}$ is the proper motion of the barycenter, ω is the argument of periapse, and f is the true anomaly, as shown in Figure 1. For the secondary,

$$K_2 = \frac{2\pi}{T}\frac{M_1}{M_1+M_2}\frac{a\sin I}{\sqrt{1-e^2}}, \tag{5}$$

with T the period of the orbit, a the semi-major axis of the elliptical orbit, and e the eccentricity. We solve for the radial velocity for both binary components, v_{r1} and v_{r2}, using $K_1 = qK_2$ for binary mass ratio $q \equiv M_2/M_1 \leqslant 1$. We introduce an additional variable $f_L \equiv L_2/(L_1+L_2)$, the luminosity ratio, and assume that emission from both black holes share the same spectral index α.

Gaudi (2010) reviews the fundamental concepts of microlensing. The characteristic scale of gravitational lensing is the angular Einstein radius,

$$\theta_E \equiv \left(\frac{4GM}{D_{\rm rel}c^2}\right)^{1/2}, \tag{6}$$

where $D_{\rm rel}^{-1} \equiv D_l^{-1} - D_s^{-1}$, D_l and D_s are the distances to the lens and source, respectively, and M is the mass of the lens. For binary self lensing, $D_{\rm rel}$ is simply the time-dependent distance between the two binary components along the line of sight (separation in the Z-direction) divided by the squared distance to the binary. A strong lensing event occurs when the source is within one Einstein radius of the lens. The width of the lensing flare depends on the orbital separation relative to the Einstein radius. Defining $u = \delta/\theta_E$, for angular separation δ between lens and source, we may write the magnification due to gravitational lensing as,

$$A(u) = \frac{u^2+2}{u\sqrt{u^2+4}}. \tag{7}$$

To calculate the flux from what we refer to as our Doppler + self-lensing model, we write,

$$(1+\Delta_{\rm Doppler})(1+\Delta_{\rm lensing}) = (1-f_L)D_1^{3-\alpha}A_1 + f_L D_2^{3-\alpha}A_2. \tag{8}$$

where D_1 (D_2) is the Doppler factor due to the line of sight velocity of the primary (secondary), and A_1 (A_2) is the lensing magnification factor when the secondary (primary) acts as the lens. The Doppler + self-lensing flare model has 10 parameters, listed in Table 1.

We use a Python implementation of Goodman & Weare's Affine Invariant Markov chain Monte Carlo (MCMC) Ensemble sampler (Goodman & Weare 2010), emcee (Foreman-Mackey et al. 2013), to fit our Doppler + self-lensing model to the light curves. We maximize the likelihood function,

$$\ln p(y|\{x_i\}) = -\frac{1}{2}\sum_n \left[\frac{(y_n - m_n)^2}{\sigma_n^2} + \ln\sigma_n^2\right], \tag{9}$$

where $\{x_i\}$ is our set of 10 variables, y_n is the light curve data, m_n is the model given $\{x_i\}$, and σ_n is the photometric error. For Ark 120 we use published errors on each data point for σ_n. For Spikey, we bin the light curve data in bins of ~ 0.5 days during the spike and bins of ~ 9 days around the spike, and use the standard deviation of each bin for the error σ_n. This is done to favor models that fit the flare as opposed to just the Doppler part of the light curve. We assume the noise on the Kepler photometric data to be Gaussian. For both Ark 120 and Spikey, the light curves are fit by the Doppler + self-lensing model using emcee to find the 10 parameters and their uncertainties listed in Table 1.

For the more promising Doppler + self-lensing candidate, Spikey, we again use emcee to fit the DRW model (Eq. 3) to the light curve to recover an additional two parameters, τ and SF_∞, from which we can also calculate $\sigma = \mathrm{SF}_\infty/\sqrt{2}$. For modeling a DRW process we follow (Kozłowski et al. 2010) and use the likelihood function,

$$\mathcal{L}_{\rm DRW} = |\mathrm{Cov}|^{-1/2}\left|L^T\mathrm{Cov}^{-1}L\right|^{-1/2}\exp\left(-\frac{\boldsymbol{Y^T}(\mathrm{Cov})^{-1}\boldsymbol{Y}}{2}\right). \tag{10}$$

Here L is a vector of ones with length equal to the number of data points. Cov is the time-domain covariance matrix comprised of DRW and photometric noise contributions, given by,

$$\mathrm{Cov}_{ij} = \sigma^2\exp\left[\frac{-|t_i - t_j|}{(1+z)\tau}\right] + \sigma_n^2\delta_{ij}, \tag{11}$$

where δ_{ij} is the Kronecker-Delta. The vector of residuals, $\boldsymbol{Y} = \boldsymbol{O} - \boldsymbol{M}$, is constructed from the observed flux $\boldsymbol{O}$ and flux predicted in the model $\boldsymbol{M}$.

We perform basic model selection by applying the DRW model to two different versions of the light curve: 1) the unadjusted light curve and 2) the model subtracted light curve. In the second case, the maximum-likelihood Doppler + self-lensing model is subtracted before sampling the posterior. To assess which of the models is favored by the data, we calculate the Bayesian Information Criterion (BIC) for each model and compare,

$$\mathrm{BIC} = \mathrm{k}\ln(\mathrm{N}) - 2\ln(\mathcal{L}_{\rm max}), \tag{12}$$

where k is the number of model parameters (12 for Doppler + self-lensing + DRW, 2 for DRW only), N is the number of data points, and $\mathcal{L}_{\rm max}$ is the maximum likelihood for a given model. A model with a lower BIC is favored, with BIC differences of $\gtrsim 6$ being significant.

3.2 Model Light Curves

D18 describe self-lensing as a unique signature of accreting SMBHBs. They show that self-lensing is expected in a few to tens of

		Ark 120		**Spikey**	
Parameter	Meaning	Prior Range	Parameters	Prior Range	Parameters
v_z [c]	velocity of barycenter along line of sight	[-1, 1]	$0.074^{+0.150}_{-0.063}$	[-1, 1]	$0.000^{+0.002}_{-0.003}$
ω [rad]	argument of periapse	[0, 2π]	$4.776^{+1.514}_{-1.144}$	[0, 2π]	$1.477^{+0.088}_{-0.081}$
e	eccentricity	[0, 1]	$0.081^{+0.098}_{-0.058}$	[0, 1]	$0.524^{+0.042}_{-0.043}$
T [yrs]	period	[18, 25]	$19.527^{+0.635}_{-0.594}$	[0, 3]	$1.144^{+0.031}_{-0.029}$
$\cos I$ [rad]	inclination	[-1, 1]	$0.281^{+0.482}_{-0.997}$	[-1, 1]	$0.140^{+0.027}_{-0.022}$
$\log(M_1/M_\odot)$	mass of primary BH	[5,11]	$9.859^{+0.714}_{-0.728}$	[5,11]	$7.4^{+0.2}_{-0.2}$
$\log(M_2/M_\odot)$	mass of secondary BH	[5,11]	$6.778^{+2.024}_{-1.278}$	[5,11]	$6.7^{+0.5}_{-0.7}$
f_L	luminosity ratio	[0,1]	$0.654^{+0.239}_{-0.287}$	[0,1]	$0.89^{+0.08}_{-0.14}$
t_0 [yrs]	arbitrary reference time	[-10, 30]	$23.167^{+4.536}_{-3.559}$	[-3, 3]	$1.693^{+0.032}_{-0.029}$
α	spectral index	[-6, 6]	$-1.555^{+2.180}_{-2.729}$	[-4, 4]	$2.09^{+0.18}_{-0.29}$

Table 1. Recovered model parameters, uncertainties and assumed priors. All values are in the rest frame of the source. Here we quote parameter values derived from the 50%, 16%, and 84% quantile estimates, see the Appendix. The results for Spikey (Ark 120) utilize the last 20,000 (2,000) steps of the MCMC walker chains.

percent of accreting SMBHBs, depending on binary parameters and assuming a circular orbit throughout. They compare lensing flares for different mass ratios and find that for extreme mass ratio cases $q \lesssim 0.05$, a significant lensing flare occurs only as the secondary passes behind the more massive primary. For larger mass ratios, a second lensing flare can occur as the primary passes behind the secondary, assuming the primary is accreting as well.

Motivated by the light curves of the two systems studied in this work, we extend the lensing model for a wider range of situations. In particular, we focus here on the dependence on two new parameters, which have not been previously discussed for Doppler + self-lensing models: the eccentricity e and the argument of periapse ω. In Figure 2, we show light curves for four example binaries with inclination $I = 87^\circ$ with varying e and ω, for $M_1 = 5 \times 10^8\ M_\odot$, $M_2 = 5 \times 10^7\ M_\odot$ ($q = 0.1$), $T \approx 20$ years, and $f_L = 0.7$, chosen to allow a second lensing flare to appear (assuming that both black holes are accreting). In plotting the light curves, we shift the light curves along the x-axis to align the primary lensing flares (where we refer to the primary lensing flare as the highest magnification flare generated when the primary acts as the lens). For circular orbits, the line-of-sight conjunctions, which correspond to the peaks of the lensing spikes, always coincide with the average flux with no Doppler boost because of the vanishing line-of-sight velocity. We show in Figure 2 that for $e > 0$, this is only true if $\omega = 90^\circ$ or 270°, for which the binary reaches periapse at its northmost or southmost distance from the plane of reference, respectively. The lensing spike is offset from the average flux for all other values of ω. When $\omega = 0^\circ$ or 180°, the binary reaches periapse when it is crossing the plane of reference from South to North or North to South, respectively.

For highly eccentric orbits, the shape of the light curve and flare magnification can vary dramatically with the argument of periapse ω. This is because the Einstein radius (Eq. 6), which sets the flare magnification and width, depends on the line of sight projected distance between the lens and source through the binary orbit, which in turn changes with both e and ω.

For eccentric orbits, the orbital velocity of both binary components is faster at periapse and slower at apoapse than for a circular orbit with the same period. Hence the widest flares occur during apoapse conjunctions and the narrowest occur at periapse conjunctions. At $\omega = 270^\circ$, the secondary is lensed at apoapse and the primary is lensed at periapse, resulting in the widest primary flares and narrowest secondary flares. In contrast, at $\omega = 90^\circ$, the secondary is lensed at periapse and the primary is lensed at apoapse, resulting in the narrowest primary flares and widest secondary flares. For ω near 0° or 180°, both lensing flares occur between the apoapse and periapse, but closer to the periapse, resulting in relatively narrow flares.

The binary components in an eccentric orbit have larger (smaller) separation at apoapse (periapse) than a binary with the same orbital period on a circular orbit. This has two consequences for the magnification. On one hand, lensing events peaking at periapse will have $\propto \sqrt{(1+e)/(1-e)}$ times smaller Einstein radii than those peaking at apoapse. On the other hand, the angular separation of source and lens is a factor of $\propto (1+e)/(1-e)$ larger at apoapse than it is at periapse. Hence, the strongest lensing flares occur when the secondary passes behind the primary at periapse; the weakest when the primary passes behind the secondary at apoapse.

This combined behaviour can be seen in the top right and bottom panels of Figure 2. The $\omega = 90^\circ$ curve denotes orbits where the secondary passes behind the primary at periapse, yielding the highest-magnification, narrowest primary lensing flares. During the same orbit, the primary is lensed by the secondary at apoapse, yielding the widest, lowest magnification secondary lensing flares. The opposite case yielding the widest, lowest magnification primary flares and the narrowest highest magnification secondary flares is seen for the $\omega = 270^\circ$ case.

As is well known, the lens mass and binary inclination can also change the width and magnification of the lensing flare. Hence, we expect the eccentricity to add further degeneracy in fitting for these parameters in the next section.

4 RESULTS

4.1 Ark 120

Figure 3 shows the optical light curve for Ark 120, overlaid with the maximum-likelihood Doppler + self-lensing model light curve in blue. Table 1 lists the 50%, 16%, and 84% quantile parameter values recovered by the MCMC posterior sampling. In green, we plot model realizations for 0.95 * (number of walkers) sets of parameters randomly drawn from the emcee samples to represent the uncertainty in the model.

For this fit, emcee was run for 20,000 steps with 500 walk-

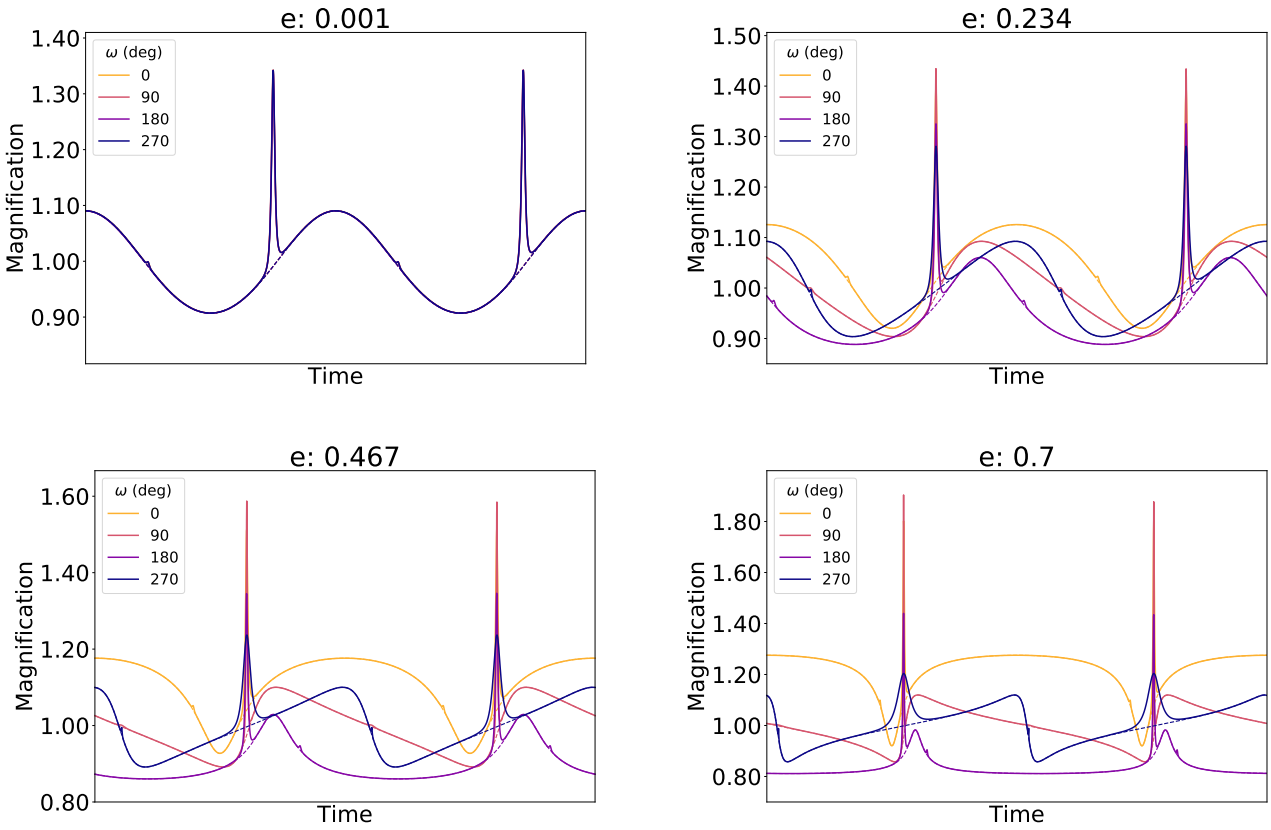

Figure 2. Example light curves for $q \equiv M_2/M_1 = 0.1$, $f_L = 0.7$, $I = 87°$, fixed eccentricity e in each subplot, and varying argument of periapse ω. Parameters are chosen to allow for a second lensing flare to appear. Dotted lines follow the light curve if there were no lensing flares. Light curve traces are shifted along the x-axis to align the primary lensing flares in each plot.

ers. Analysis is carried out on the final 10% of the chains, well after convergence. The Doppler-boost model requires a negative (or small positive) α due to the long period and large amplitude. Publicly available optical spectra, covering wavelengths around the $H\beta$ line, not far from the V band, exist from 1976 to 2017 (Capriotti et al. 1982; Korista 1992; Stanic et al. 2000; Peterson et al. 1998; Doroshenko et al. 2008). We use four spectra from Korista (1992), dating from 1981 through 1984, and find that the power-law component of the continuum is best fit with an average spectral index of $\alpha = 2.36$. For this larger measured value of α, a larger binary mass and smaller mass ratio at fixed orbital period could explain the large amplitude of Doppler-boost variations. Hence, we repeat our analysis, but with α fixed to be 2.36. We find $\log[M_1/M_\odot] \approx 6.5^{+1.4}_{-0.9}$ and $\log[M_1/M_\odot] \approx 10.5^{+0.4}_{-0.7}$, with the other parameters largely unchanged. This suggest a primary mass approaching the limit of expected and known supermassive black hole masses, but not so large that the Doppler model is ruled out. While not theoretically impossible, this large mass is at odds with a measured value of the central compact mass within Ark 120. Broad-line-width measurements provide an estimate of $M_{\rm BH} = (2.6 \pm 0.2) \times 10^8 M_\odot$ (Li et al. 2019). However, systematic uncertainties in central mass estimation from broad-line measurements, as well as the possibility of a time variable spectral slope, could alleviate the above consistencies. Furthermore, we note that the Kepler bandpass ranges from 420 to 900 nm, while the spectra from Korista (1992) only covered 450 to 550 nm.

Hence, based on the mass inconsistency and in light of these caveats, we disfavor but do not rule out the Doppler hypothesis for Ark 120. Further measurements of the spectral slope and central mass in Ark 120 as well as further optical monitoring can elucidate these issues in the future.

Even in the case that the Doppler-boost scenario is viable, we find that model realizations exhibiting a significant lensing flare are not favored. This can be seen more quantitatively by comparing the BIC (Eq. 12) computed for the Doppler + self-lensing model to the BIC computed for the Doppler-only model. The difference in BIC between the two is consistent with zero, as is expected since both models have the same number of parameters, and find a similar best-fit.

Outside of the Doppler + self-lensing, scenario, we note that periodicity due to time variable accretion coupled with lensing is not ruled out, but is more difficult to test as there is no predicted correlation between the sinusoidal variability and the lens flare; the lens flare could occur at any phase and amplitude relative to the sinusoidal variability. Regardless, observed periodically recurring flares in Ark 120 would warrant further investigation into this possibility.

4.2 Spikey

Figure 4 shows the optical light curve for Spikey overlaid with the maximum-likelihood Doppler + self-lensing model light curve in blue, and Table 1 lists the 50% quantile parameters values with errors quoted from the 16% and 84% values. Again, in green we

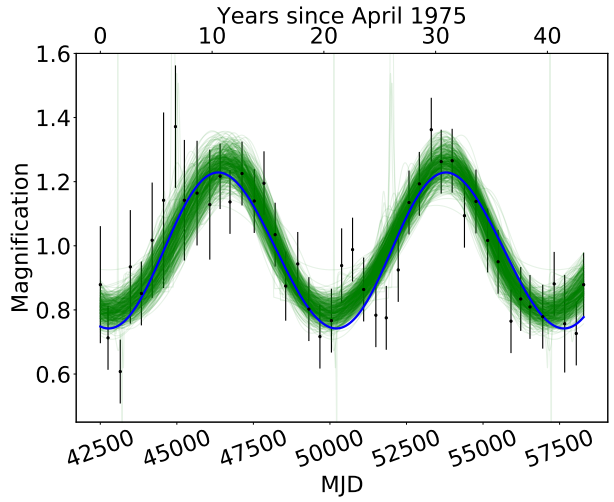

Figure 3. Optical light curve for Ark 120, overlaid with the maximum-likelihood Doppler + self-lensing model light curve in blue, and model realizations for 0.95 * (number of walkers) sets of parameters randomly drawn from the set of samples to represent the 95% uncertainty, in green. For this fit, emcee was run for 20,000 steps with 500 walkers.

plot model realizations for 0.95 * (number of walkers) sets of parameters randomly drawn from the emcee samples to represent the 95% uncertainty. emcee was run for 50,000 steps with 500 walkers. The overall shape of Spikey's light curve, without lensing, is non-sinusoidal, suggesting a non-zero eccentricity. The narrowness of the spike, with a width of approximately 10 days, can be due to the Einstein radius being small compared to the orbital separation. In the right panel of Figure 4 we see that the symmetric shape of the spike is remarkably close to the symmetric Paczynski-curve shape predicted in the Doppler + self-lensing flare model.

An optical spectrum was obtained for Spikey on June 25, 2012, from which a power-law slope is measured to be $\alpha \sim -0.12$.[2] This is not consistent with our recovered α parameter for Spikey (Table 1); however, the error on the measured value could be large. Otherwise the discrepancy could arise from a variable spectral slope within the Doppler + self-lensing model.

To further investigate the plausibility of the Spikey Doppler + self-lensing model, we calculate the BIC (Eq. 12) for DRW models of the light curve with and without the Doppler + self-lensing model (Eq. 4 through 7) subtracted, as described in §3.1. This allows us to assess whether including the Doppler + self-lensing model improves the fit relative to the DRW model alone.

We find a strong difference in the BIC between the two models of ≈ 190, favoring the Doppler + self-lensing + DRW model over the purely DRW model. The 50% quantile likelihood DRW parameters, with errors from the 16% and 84% quantile values, for the DRW-only model are $\tau = 586^{+289}_{-337}$ days and $\mathrm{SF}_\infty = 0.052^{+0.012}_{-0.018}$ mag, and for the Doppler + self-lensing subtracted light curve, $\tau = 434^{+397}_{-365}$ days and $\mathrm{SF}_\infty = 0.034^{+0.013}_{-0.020}$ mag. We note that the maximum likelihood parameters are slightly different due to the non-Gaussian nature of the posterior. For the Doppler + self-lensing subtracted light curve, a peak in the posterior probability is found at smaller values of $\tau = 31$ days and $\mathrm{SF}_\infty = 0.01$ mag. For the un-subtracted light curve, no such peak is found and the maximum-likelihood parameters are $\tau = 123$ days and $\mathrm{SF}_\infty = 0.024$ mag. This test confirms that it is not likely for the DRW process to generate such a sharp feature on short timescales. The priors are chosen so that τ encompasses the temporal baseline of the data $\tau = [0, 10^3]$ days while SF_∞ is essentially unbounded $\mathrm{SF}_\infty = [0, 200]$ mag.

In Figure 6, we plot the PSD(f) for the data with and without the Doppler + self-lensing model subtracted. With the Doppler + self-lensing model subtracted, the PSD(f) begins to show a break, as described in §3.1, while previously, no break was found (Smith et al. 2018). The break appears presumably because of the additional power at the frequency of $f \sim 1/\mathrm{yr}$ contributed by the Doppler modulation.

The most obvious way to test the self-lensing SMBHB hypothesis for Spikey is to look for periodically recurring lensing flares. In Figure 5, we extend the Doppler + self-lensing model for Spikey's light curve to show future lensing flares through 2020. Three predicted lensing flares could have occurred since Kepler observed Spikey. The next putative flares are set to occur in April 2020 and July 2022. We discuss the possibility of detecting these flares in archival and future observations below.

5 DISCUSSION

We note that our lensing model assumes a point source, while the optical emitting region is known to have a finite size of a few hundred gravitational radii (Paczynski 1977; Roedig et al. 2014; Artymowicz & Lubow 1994). Assuming black-body emission from a steady-state, optically thick accretion disk, D18 compute when the wavelength-dependent size of an accretion-disk source becomes of order the size of the Einstein radius, and hence falls within the finite-sized source regime. Using Eq. (9) of D18 with the maximum-likelihood Spikey binary parameters, 10% accretion efficiency at the Eddington limit (consistent with the luminosity and mass estimate for Spikey), and considering the $420 - 900$ nm Kepler bandpass, we find that the ratio of effective disk size to Einstein radius ranges from $\sim 0.3 - 0.9$. Hence, the putative accretion disk around the lensed binary component may act like a finite-sized source at the long-wavelength end of the Kepler band.

As D18 show, a finite-sized source results in a lower magnification than for a point-source, and in extreme cases, a wider lensing flare. This could affect the mass and eccentricity parameter estimation computed here. However, as evidenced by Figure 5 in D18, we do not expect this effect to be large, especially in the marginally finite-sized source regime in the Kepler band into which Spikey falls.

While a useful estimate of the relevant lensing regime, the above is based on one source model which would itself depend on the inclination of the disk to the line-of-sight. Whether or not the source must be treated as a finite source depends on the unknown emission region structure in the lensed accretion flow. However, we note that the behavior of finite source lensing and the propensity of accretion flows to be hotter closer to the central compact object suggest that finding wider, lower magnification symmetric flares at longer wavelengths is indicative of lensing. If the binary self-lensing hypothesis could be confirmed for Spikey, then multi-

[2] The optical spectrum was obtained with the KAST double spectrograph on the Shane 3-m telescope at Lick Observatory. To obtain the spectral index in this region, the two strong emission lines (C III λ1909 and Mg II λ2799) are masked out and the continuum is fit with a linear model using a least-squares method.

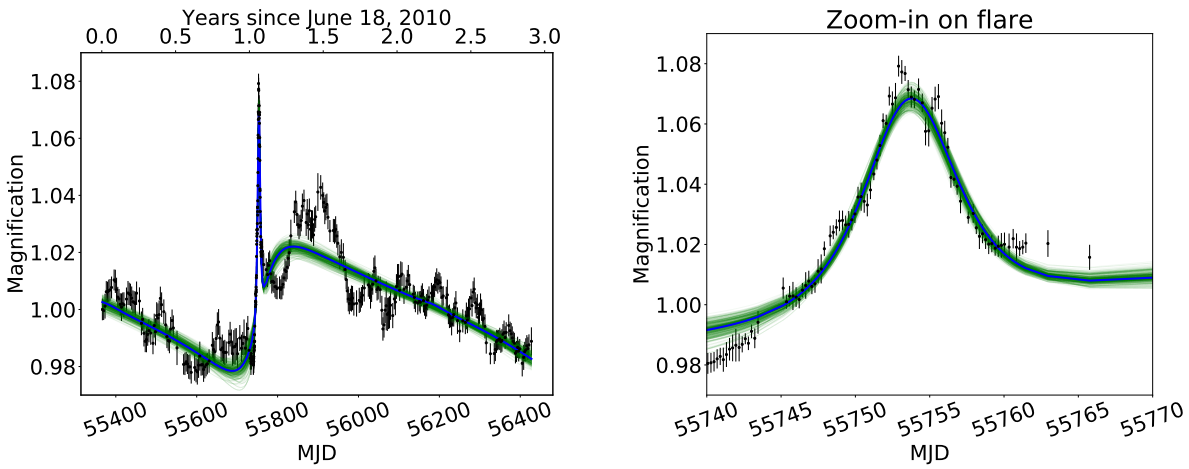

Figure 4. Optical light curve for Spikey, overlaid with the maximum-likelihood Doppler + self-lensing model, in blue, and 95% uncertainty, in green. Here, emcee was run for 50,000 steps with 500 walkers. On the right we zoom-in on the lensing flare.

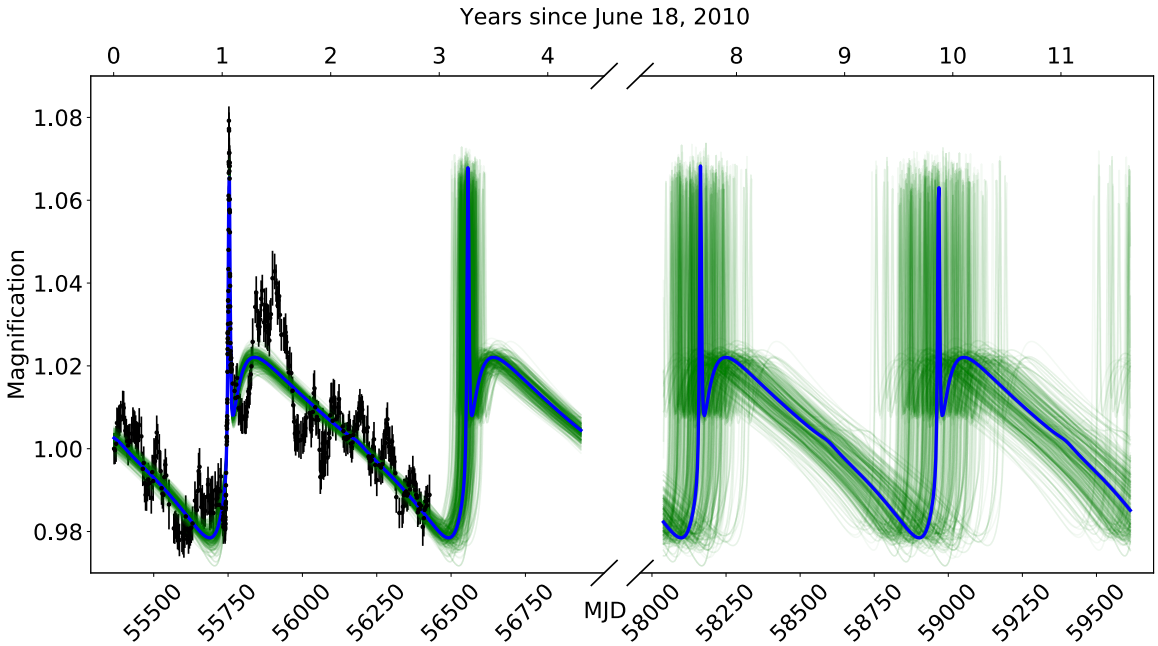

Figure 5. Optical light curve for Spikey, with overlaid maximum-likelihood Doppler + self-lensing model and uncertainty extended to show predicted flares in September 2013, February 2018, and April 2020. Cut out of the plot is the predicted flare in December 2015. A July 2022 flare is also predicted.

wavelength observations of a flare would teach us a great deal about the emission region geometry.

Finally, our model for Spikey predicts a relativistic orbital precession of the argument of periapse by $\sim 1.3^\circ$ per orbit, which would alter the timing of the next flare by approximately 1.5 days per orbit. While this does not greatly affect the prediction for the time of the next flare, it does present the exciting prospect of tracking general relativistic effects on the orbit with self-lensing.

5.1 Other data and first X-ray observations of Spikey

We have used only Kepler data in vetting the Doppler + self-lensing model for Spikey. While other data exists, none of it has a high enough cadence or photometric precision to further constrain or rule out our model. Figure 7 shows optical data from the Zwicky Transient Facility (ZTF; which is unfortunately sparse due to positioning of Spikey on a chip gap, Bellm 2014) and IR data from the Wide-field Infrared Survey Explorer (WISE). In addition, the TESS satellite has observed Spikey during the months of June through September 2019 and Gaia has observed Spikey since 2015, and will continue to do so.

We additionally found data from the ASAS-SN photometric database; however, it is likely that the PSF for ASAS-SN is too large to isolate emission from Spikey alone. The data consists largely of upper limits except for a number of widely varying detections ranging three orders of magnitude in brightness. As there are multiple stars in this magnitude range near Spikey, and as Spikey is near the magnitude limit for ASAS-SN ($\sim 18^{\rm th}$ magnitude), we do not include these data.

Future planned observations tailored to observing a repeating

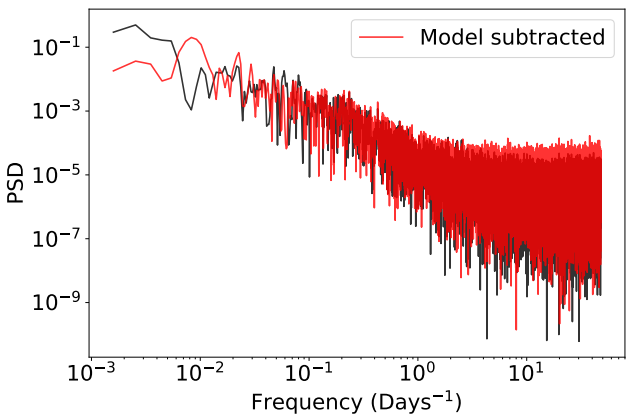

Figure 6. PSD(f) for Spikey data with (red) and without (black) the Doppler + self-lensing model subtracted. With the model subtracted, the PSD(f) begins to show a break, while without the model subtracted, no break was found.

flare, as well as further data from ZTF, TESS, and Gaia, will be vital in ruling out or confirming the Doppler + self-lensing scenario for Spikey. Gaia epoch data, when it is released, will likely sample Spikey's light curve with high enough cadence to rule out or confirm the self-lensing scenario. With this, as well as the benefits of multi-wavelength (especially X-ray) observations for confirming and learning from the self-lensing scenario in mind, we have obtained X-ray observations of Spikey with Swift and have scheduled observations with Chandra.

Initial X-ray observations of Spikey were performed with Swift during Cycle 15 on 2019 March 16 and 2019 June 22 for 14.4 ks and 14.0 ks, respectively. The observations were intended to measure the X-ray properties of the source and establish X-ray light curve data. Spikey was confirmed to be a moderately bright X-ray source with an average count rate of $0.01\,\mathrm{cts\,s^{-1}}$ with the Swift X-Ray Telescope (XRT) instrument. XRT spectra were fit with a `phabs·zpowerlaw` model using Cash statistics (cstat) to determine the spectral slope α and 0.5–7.0 keV flux $F_{0.5-7.0\,\mathrm{keV}}$ in each observation, where the parameters are defined the same as in Section 3. The Galactic column density was set to $n_\mathrm{H} = 6.8 \times 10^{20}\,\mathrm{cm^2}$ as extrapolated from Dickey & Lockman (1990). Best-fit results for the March 16 observation were $\alpha = 0.56 \pm 0.12$ and $F_{0.5-7.0\,\mathrm{keV}} = 6.2 \pm 1.0 \times 10^{-13}\,\mathrm{erg\,cm^{-2}\,s^{-1}}$, while the June 22 best-fit results were $\alpha = 0.67 \pm 0.18$ and $F_{0.5-7.0\,\mathrm{keV}} = 4.5 \pm 0.9 \times 10^{-13}\,\mathrm{erg\,cm^{-2}\,s^{-1}}$. The flux estimates indicate a decrease in brightness over time, which is broadly consistent with the decreasing intensity expected for Spikey during this period.

This first detection of X-rays from Spikey is promising for upcoming Chandra observations presently scheduled for the predicted flaring period in 2020. These observations will be sensitive enough to detect a 5% increase in brightness, and hence detect the putative next flare. Detection of a repeating flare would provide very strong evidence for the SMBHB and self-lensing scenario, and importantly, non-detection of a flare will remove evidence for the SMBHB hypothesis.

6 CONCLUSIONS

We extended previous Doppler + self-lensing models to include eccentric orbits, motivated by searches for sub-pc separation SMBHBs via unique periodic signatures in their continuum light curves caused by the relativistic Doppler boost and gravitational lensing of an accreting binary. We used these models to investigate the optical light curves of two intriguing quasars, Ark 120 and KIC 11606854 (Spikey).

The sinusoid-like light curve of Ark 120 suggests a binary candidate with a 20-yr period; two prominent flares suggest an eccentric orbit with lensing. We find no evidence that a SMBHB Doppler + self-lensing model can describe the flares observed in the Ark 120 light curve. While we do not rule out a Doppler boost only model for Ark 120, it is disfavoured as our models predict a binary mass that is two orders of magnitude larger than the central mass estimate from single-epoch broad-line measurements.

The light curve of Spikey appears to be non-sinusoidal if periodic and has a narrow symmetric spike, suggesting an eccentric orbit and lensing. We fit our Doppler + self-lensing model to the data and find parameters that suggest a total binary mass of $M_\mathrm{tot} \approx 3\times \sim 10^7 M_\odot$ and rest-frame orbital period $T = 418$ days. We find that the combination of Doppler + self-lensing + DRW model provides a better fit for the variability than the DRW model alone. This interpretation can be tested by monitoring Spikey for periodic behavior and recurring spikes, the next of which are set to occur in April 2020 and July 2022 (Figures 5 and 7).

Because future searches for flares may be even cleaner in X-rays, since X-ray emission is more compact and can be magnified by a larger factor, we have obtained the first X-ray data on Spikey using the Swift observatory. Though not taken during a predicted flaring period, these data show that Spikey is a bright source of X-rays; hence, future X-ray observations have the opportunity to detect the next lensing flare predicted here. The lack of a flare within the predicted windows would rule out the SMBHB self-lensing hypothesis while the detection of a repeating symmetric flare would be the most definitive evidence to date for a sub-pc separation supermassive black hole binary.

ACKNOWLEDGEMENTS

The authors thank Alberto Sesana, Thomas Kupfer, and Matthew Graham for useful discussions. DJD acknowledges support from NASA through Einstein Postdoctoral Fellowship award number PF6-170151 and funding from the Institute for Theory and Computation Fellowship. ZH acknowledges support from NSF grant 1715661 and NASA grants NNX17AL82G and 80NSSC19K0149. KLS acknowledges support from Einstein Postdoctoral Fellowship award number PF7-180168. MC acknowledges support from the National Science Foundation (NSF) NANOGrav Physics Frontier Center, award number 1430284. Funding for this work was partially provided through Swift proposal #1518206. This paper includes data collected by the Kepler mission. Funding for the Kepler mission is provided by the NASA Science Mission directorate.

REFERENCES

Artymowicz P., Lubow S. H., 1994, ApJ, 421, 651
Begelman M. C., Blandford R. D., Rees M. J., 1980, Nature, 287, 307

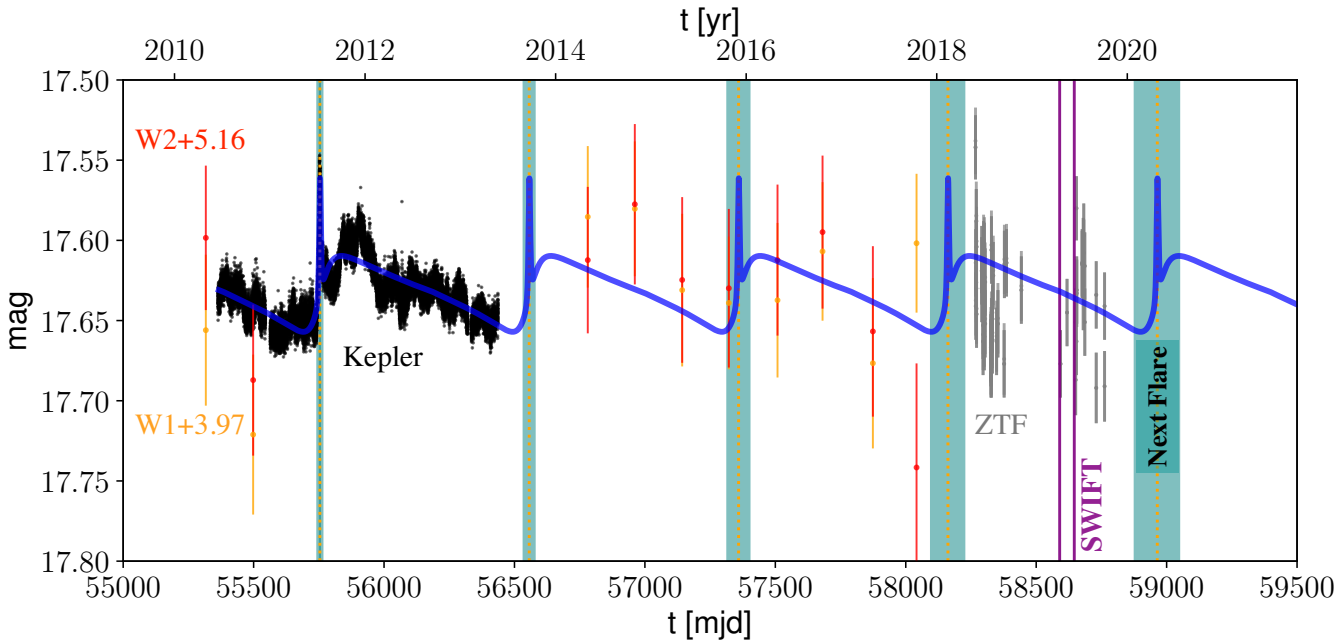

Figure 7. Archival data on Spikey along with the dates of the first X-ray data obtained with Swift (purple vertical lines). Shaded teal regions are the projected dates of lensing flares, the next (at writing) being in 2020. Not shown are unreleased TESS and Gaia observations as well as proposed Chandra observations during the projected next flare.

Bellm E., 2014, in Wozniak P. R., Graham M. J., Mahabal A. A., Seaman R., eds, The Third Hot-wiring the Transient Universe Workshop. pp 27–33 (arXiv:1410.8185)

Bowen D. B., Mewes V., Noble S. C., Avara M., Campanelli M., Krolik J. H., 2019, ApJ, 879, 76

Capriotti E. R., Foltz C. B., Peterson B. M., 1982, ApJ, 261, 35

Carini M. T., Ryle W. T., 2012, ApJ, 749, 70

Charisi M., Bartos I., Haiman Z., Price-Whelan A. M., Graham M. J., Bellm E. C., Laher R. R., Márka S., 2016, MNRAS, 463, 2145

Charisi M., Haiman Z., Schiminovich D., D'Orazio D. J., 2018, Monthly Notices of the Royal Astronomical Society, 476, 4617–4628

Comerford J. M., Schluns K., Greene J. E., Cool R. J., 2013, ApJ, 777, 64

Cuadra J., Armitage P. J., Alexander R. D., Begelman M. C., 2009, MNRAS, 393, 1423

D'Orazio D. J., Di Stefano R., 2018, MNRAS, 474, 2975

D'Orazio D. J., Di Stefano R., 2019, arXiv e-prints, p. arXiv:1906.11149

D'Orazio D. J., Haiman Z., MacFadyen A., 2013, MNRAS, 436, 2997

D'Orazio D. J., Haiman Z., Duffell P., Farris B. D., MacFadyen A. I., 2015a, MNRAS, 452, 2540

D'Orazio D. J., Haiman Z., Schiminovich D., 2015b, Nature, 525, 351

D'Orazio D. J., Haiman Z., Duffell P., MacFadyen A., Farris B., 2016, Monthly Notices of the Royal Astronomical Society, 459, 2379

Dickey J. M., Lockman F. J., 1990, ARA&A, 28, 215

Doroshenko V. T., Sergeev S. G., Pronik V. I., 2008, Astronomy Reports, 52, 442

Dotti M., Sesana A., Decarli R., 2012, Advances in Astronomy, 2012, 940568

Edelson R., Malkan M., 2012, ApJ, 751, 52

Farris B. D., Duffell P., MacFadyen A. I., Haiman Z., 2014, ApJ, 783, 134

Foreman-Mackey D., 2016, The Journal of Open Source Software, 24

Foreman-Mackey D., Hogg D. W., Lang D., Goodman J., 2013, PASP, 125, 306

Gaudi B. S., 2010, arXiv e-prints, p. arXiv:1002.0332

Goodman J., Weare J., 2010, Communications in Applied Mathematics and Computational Science, Vol.~5, No.~1, p.~65-80, 2010, 5, 65

Graham M. J., et al., 2015, MNRAS, 453, 1562

Hayasaki K., Mineshige S., Sudou H., 2007, Publications of the Astronomical Society of Japan, 59, 427

Hughes P. A., Aller H. D., Aller M. F., 1992, ApJ, 396, 469

Kasliwal V. P., Vogeley M. S., Richards G. T., 2015, MNRAS, 451, 4328

Korista K. T., 1992, ApJS, 79, 285

Kormendy J., Ho L. C., 2013, ARA&A, 51, 511

Kozłowski S., et al., 2010, ApJ, 708, 927

Li Y.-R., et al., 2019, ApJS, 241, 33

Liu T., et al., 2019, arXiv e-prints, p. arXiv:1906.08315

MacFadyen A. I., Milosavljević M., 2008, ApJ, 672, 83

MacLeod C. L., et al., 2010, ApJ, 721, 1014

Muñoz D. J., Lai D., 2016, ApJ, 827, 43

Murray C. D., Correia A. C. M., 2010, Keplerian Orbits and Dynamics of Exoplanets (arXiv:1009.1738)

Paczynski B., 1977, ApJ, 216, 822

Peterson B. M., Wanders I., Horne K., Collier S., Alexander T., Kaspi S., Maoz D., 1998, PASP, 110, 660

Richstone D., et al., 1998, Nature, 395, A14

Roedig C., Krolik J. H., Miller M. C., 2014, ApJ, 785, 115

Shi J.-M., Krolik J. H., 2015, ApJ, 807, 131

Shi J.-M., Krolik J. H., Lubow S. H., Hawley J. F., 2012, ApJ, 749, 118

Smith K. L., Mushotzky R. F., Boyd P. T., Malkan M., Howell S. B., Gelino D. M., 2018, ApJ, 857, 141

Stanic N., Popovic L. C., Kubicela A., Bon E., 2000, Serbian Astronomical Journal, 162

Vaughan S., Uttley P., Markowitz A. G., Huppenkothen D., Middleton M. J., Alston W. N., Scargle J. D., Farr W. M., 2016, MNRAS, 461, 3145

7 APPENDIX

7.1 MCMC statistics

We include the assumed prior range of values in Table 1. For completeness we provide the one and two dimensional posterior distributions sampled by emcee (Foreman-Mackey et al. 2013) for our more important result, Spikey. A degeneracy between parameters M and I already exists for circular orbits. When we take into account eccentric orbits, we see additional degeneracies between e and M, and e and I, as discussed in §3. In the present case,

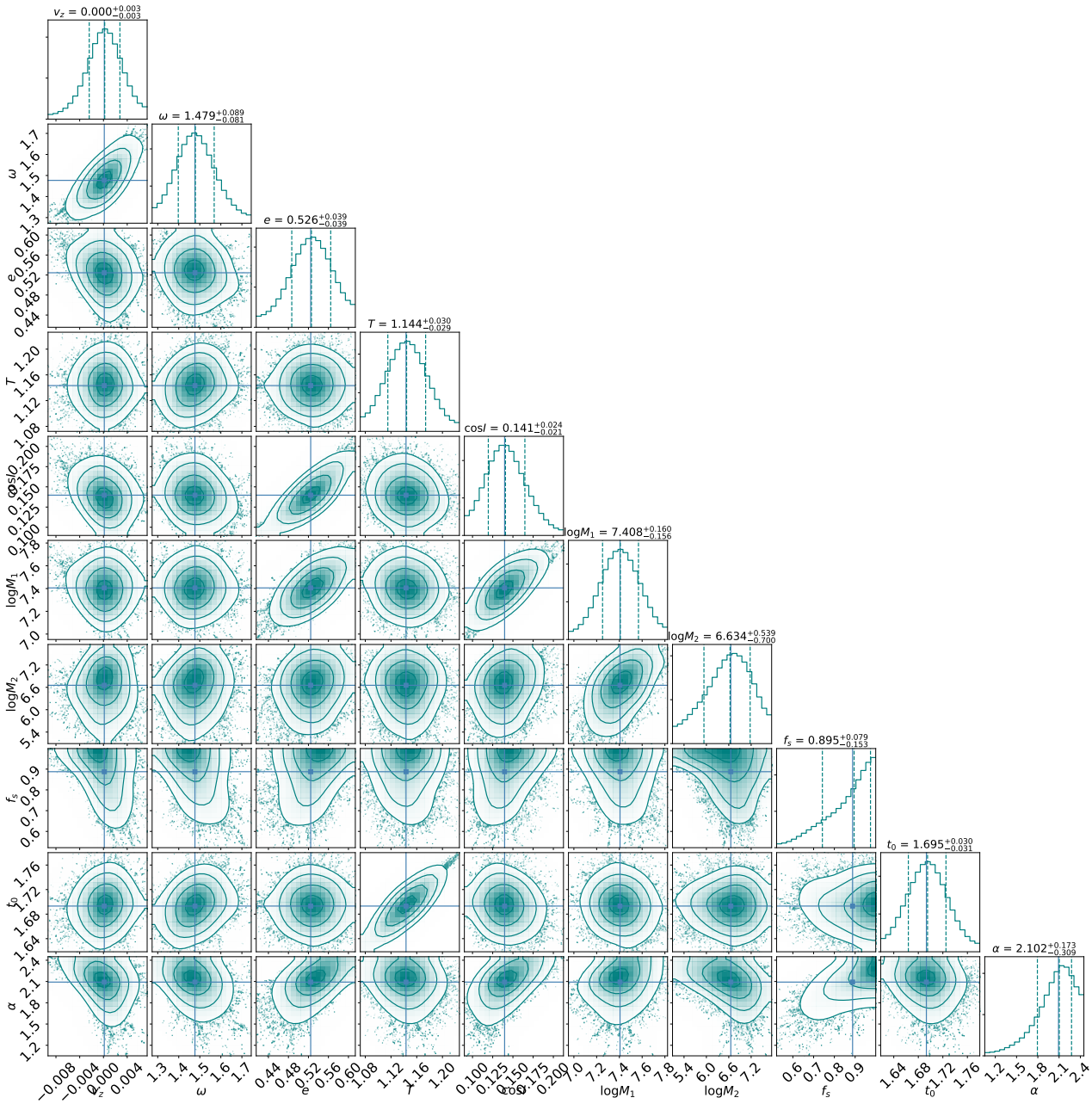

Figure 8. One and two dimensional projections of the posterior probability distributions of the parameters, for Spikey. The intersecting lines on the 2D-posterier contours signify the 50% likelihood values of the parameters, while the quoted parameters above the 1D distributions are uncertainties derived from the 50% 16%, and 84% quantile values using the last 100 steps for each walker. Compare with the maximum likelihood values listed in Table 1, along with the relevant units. Corner plot made using *corner* (Foreman-Mackey 2016).

the range of parameter values over which these degeneracies are present is small.